JOURNAL OF APPLIED ELECTROCHEMISTRY 19 (1989) 580–588

Evaluation of cathode material properties relevant to the life of Hall–Heroult cells*

M. SØRLIE

Elkem a/s, R&D Center, N-4602 Kristiansand S, Norway

H. A. ØYE

Inst. of Inorganic Chemistry, The Norwegian Institute of Technology, N-7034, Trondheim, Norway

Received August 1988; revised 4 November 1988

Proper start-up procedures and operation are extremely important for a satisfactory life of an aluminium reduction cell, but the thermomechanical and chemical properties of cathode materials relative to the design of the lining may lead to failure in an otherwise normally operated cell. The producers of cathode materials (carbon blocks, ramming paste, firebricks and insulation) usually characterize their materials well with respect to room temperature properties but it is also important to have a good understanding of materials properties under actual start-up and electrolysis conditions. Towards this goal we have adapted, improved or developed test methods which we consider important as design tools as well as for quality control of the materials. Examples of materials properties and designs that may lead to failures are given.

1. General features of the carbon cathode

Figure 1 shows, schematically, a side and end view of a cathode lining consisting of prebaked blocks with rammed seams.

1.1. *Ramming paste*

The main purpose of the ramming paste, which usually consists of an anthracitic filler and a coal tar-based binder, both in the joints and in the peripheral seam, is to fill the voids between the prebaked blocks and prevent metal and bath from penetrating into the inner parts of the cathode. A good 'weld' between the paste and the block after baking ensures a better seal and reduces the probability of liquid penetration, but is not absolutely required.

Another purpose of the rammed parts, in particular the peripheral seam, is to provide a layer which absorbs the thermal expansion of the prebaked bottom lining up to the paste baking temperature during preheating of the cell. Peripheral seams also result from the geometrical problem of fitting the blocks into the potshell when the potshell has a permanent deckplate.

The remaining paste can be hot (applied around 150° C), tepid (≈ 50° C) or room temperature paste (≈ 20° C). Room temperature or tepid pastes are rapidly becoming the dominant ramming materials used with prebaked cathode blocks. Ease of handling, environmental considerations and regulations have been the force behind the conversion from hot pastes to room temperature or tepid pastes that has taken place during the last decade. Important properties for ramming pastes that may influence potlife are: compactability, shrinkage upon baking and quality of carbon filler and binder.

1.2. *Cathode blocks*

Cathode blocks come in a variety of qualities and shapes, the latter mainly being dependent on pot design and material handling equipment available for relining operations. They may be classified as follows:

Graphitized: the whole block (aggregate and binder) consisting of graphitizable materials has been heat treated, usually to 3000° C, giving a graphitic material.

Semi-graphitized: the whole block (filler and binder) consisting of graphitizable materials has been heat treated to about 2300° C.

Semi-graphitic: the aggregate is graphitized but the

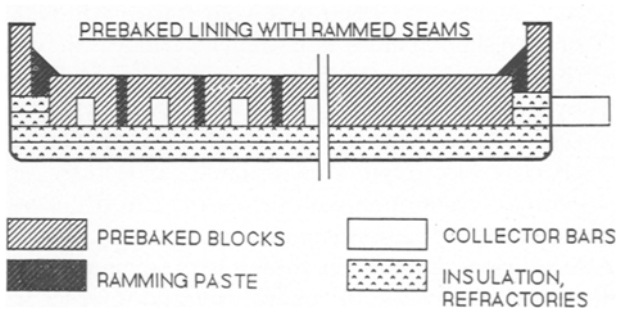

Fig. 1. Construction principles for a pot with prebaked carbon blocks and carbon paste in seams and joints.

* Paper presented at the meeting on Materials Problems and Material Sciences in Electrochemical Engineering Practice organised by the Working Party on Electrochemical Engineering of the European Federation of Chemical Engineers held at Maastricht, The Netherlands, September 17th and 18th 1987.

0021-891X/89 $03.00 + .12

block (binder coke) has only been heated to normal baking temperatures ($\simeq 1200°$ C).

Amorphous: none, or only part, of the filler material is graphitized. The block is baked to $\simeq 1200°$ C.

The amorphous carbon qualities can be further subclassified:

Gas or kiln calcined amorphous carbon: aggregate is usually anthracite (GCA) which has been evenly calcined and where no graphitization has occurred.

Electrocalcined amorphous carbon: filler material is usually anthracite (ECA) and due to the process some of the material is graphitized.

Amorphous carbon with graphitic addition (partly graphitic carbon): graphitic filler is added to the material.

Some characteristic properties (relative) of amorphous carbon blocks (anthracite) and graphitic blocks are listed in Table 1.

1.3. *Sidewall blocks*

The sidewalls of the cathode are usually made from prebaked carbon blocks, ramming paste or a combination of both. Prebaked sidewall blocks are usually manufactured from the same materials and with the same formulations as the bottom blocks, even often cut from scrap or rejects from this production, thus having similar properties. It is intended that no current pass through the sidewall, so electrical properties are therefore unimportant. Heat-conducting properties are, on the other hand, more important in the sidewall carbon than in the bottom blocks. Another very important property in the sidewall is resistance to air oxidation and attack by electrolyte and molten metal. This may be counteracted by more air oxidation-resistant carbon materials, ceramic materials or better covering of exposed areas.

Silicon carbide and silicon carbide-containing materials have for a long time been an alternate construction material for use in the sidelining; the reason why these have not been more widely used is the high cost compared to carbon.

2. Chemical reactions

The deposition of aluminium at the surface of the liquid aluminium pool is the primary cathode reaction. The solid cathode assembly (carbon materials, steel collector bars, refractory materials, insulation materials and steel shell) functions as container and conductor of electricity and should, in principle, not react with either liquid aluminium or bath. It is, however, well known that chemical surface reactions, impregnation of bath and reactions within the assembly proceed during the lifetime of a cell. In the following the secondary chemical reactions and impregnation processses in the different parts of the cathode will be discussed.

Table 1. A qualitative comparison between various properties of amorphous (anthracite) and graphitic cathode carbon blocks

	Anthracite	*Graphite*
Price	low	high
Abrasion resistance	high	low
Thermal shock resistance	high	very high
Thermal conductivity	low	high
Electrical conductivity	low	high
Strength	variable	variable
Modulus of elasticity	high	low
Resistance to Na	low	high
Crystalline stability	low	high

2.1. *Oxidation of sidelining*

Carbon is unstable towards air:

$$C(s) + O_2(g) = CO_2(g) \quad (1)$$

Air oxidation is enhanced by the presence of impurities such as V, Na, Pb and Cu and by high porosity and is inhibited by halogens, boron and phosphorus [1]. The rate of air oxidation is, of course, also enhanced by increase in temperature, making thermal conductance and insulation important design parameters.

2.2. *Formation of aluminium carbide*

The reaction between aluminium metal and carbon:

$$4Al(1) + 3C(s) = Al_4C_3(s) \quad (2)$$

is thermodynamically favoured at all temperatures of concern in electrolytic aluminium production [2]. The reaction proceeds, however, only in the presence of electrolyte and a solid layer of $Al_4Cl_3(s)$ is formed, whereupon the diffusion-controlled reaction virtually stops [3]. Solid Al_4C_3 may, however, be dissolved in the electrolyte and be reoxidized by the anode gas:

$$Al_4C_3(sol) + 9CO_2(g) = 2Al_2O_3(sol) + 12CO(g) \quad (3)$$

leading to undersaturation and dissolution of the carbide films formed. Hence a steady consumption of cathode carbon may result.

2.3. *Formation of intercalating sodium*

Neither liquid aluminium nor the cryolite melt usually wet carbon and carbon should hence be impervious to both liquids. It is nevertheless known that the carbon cathodes will be impregnated with salt; the weight of the salt in a used cathode may even exceed the weight of the remaining carbon. The initial reaction, which leads to impregnation of salts, is considered to be:

$$Al(l) + 3NaF \text{ (in cryolite)} = 3Na \text{ (in C)} + AlF_3 \text{ (in cryolite)} \quad (4)$$

The activity of Na at 1000° C above Al(l) and $Na_3AlF_6(l)$ is 0.034 [4] corresponding to a vapour pressure of Na at 970° C of 0.06 atm. From Equation 4 it is seen that the sodium activity (or pressure) will

increase with increasing cryolite ratio, CR (mol NaF/mol AlF_3).

The interaction between Na and C is enhanced by bond forming through intercalation. Although stoichiometric compounds are probably not formed in the carbon cathode, the tendency to bond formation will drive the reaction to the right. The energy driving the process is charge transfer between the diffusing atom and the π-bond system of the carbon. The Fermi level of the delocalized electrons of carbon are important in such a way that if the electron charge transfer is to the carbon (as with an electron donor, such as sodium, as intercalant), the penetration will be favoured by a low Fermi level (as found in an amorphous carbon such as GCA), while intercalation of a strong electron acceptor (such as $AlCl_3$, Br_2) will be favoured by a high Fermi level (as found in a well-crystallized graphite).

2.4. *The impregnation of liquid bath*

Due to capillary action bath impregnation takes place after the sodium front has moved through the carbon and only through the porous network formed by the volatilization and shrinkage of the binder during baking.

Compounds usually found in discarded potlinings are NaF (enriched relative to bulk composition), Al_4C_3, Na_3AlF_6, Al_2O_3, Na_2CO_3, $Na_2O \cdot 11Al_2O_3$ (β-alumina), small amounts of NaCN, AlN and Al–Fe alloys (Al_2Fe, $AlFe_3$, etc.). There is no evidence confirming that liquid aluminium penetrates the carbon lining provided that macroscopic cracks are not developed. Some of the salt deposits may be from crystallization of penetrating bath, but it is generally assumed that intercalated sodium plays a vital part in the formation of many of the above compounds. The following reactions are assumed:

Primary reaction:

$$4Na_3AlF_6(l) + 12Na(C) + 3C(s) = Al_4C_3(s) + 24NaF(l) \quad (5)$$

Increased basicity gives precipitation of β-alumina:

$$12NaF(l) + 34Al_2O_3(diss) = 3(Na_2O \cdot 11Al_2O_3)(s) + 2Na_3AlF_6(l) \quad (6)$$

Presence of air:

$$4Na_3AlF_6(l) + 12Na(C) + 3O_2(air) = 2Al_2O_3(s) + 24NaF(l) \quad (7)$$

$$4Na(C) + 3O_2(air) + 2C(s) = 2Na_2CO_3(l) \quad (8)$$

$$2Na(C) + 2C(s) + N_2(air) = 2NaCN(l) \quad (9)$$

$$2Al(l) + N_2(air) = 2AlN(s) \quad (10)$$

Reversal due to cooling:

$$Na_3AlF_6(l) + 3Na(C) = 6NaF(l) + Al(l) \quad (11)$$

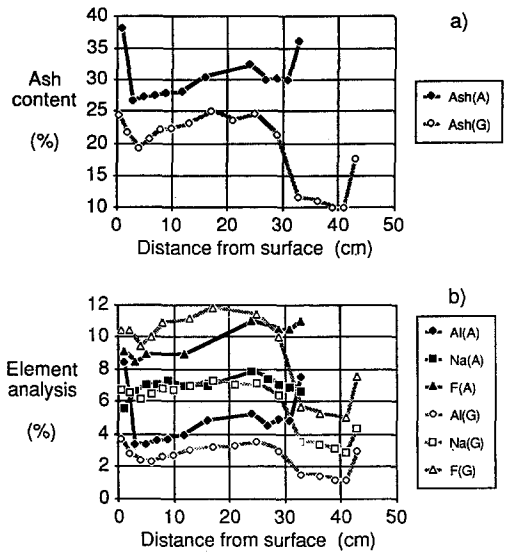

Fig. 2. Ash (a) and element (b) distribution in amorphous (A) and semi-graphitic (G) bottom blocks after 207 and 262 days of operation, respectively.

Reactions with collector bars:

$$Na_3AlF_6(l) + 3Na(C) + 3Fe(s) = AlFe_3(s) + 6NaF(l) \quad (12)$$

$$Al(l) + 3Fe(s) = AlFe_3(s) \quad (13)$$

Figure 2 shows the element distribution in two bottom blocks.

3. Physical changes during cell operation

3.1. *Thermal expansion and shrinkage*

Cathode bottom blocks are installed at ambient temperature but their operating temperature is usually between 850 and 970° C. This causes an expansion of the cathode due to the thermal effect alone. Generally the expansion is around 0.4% from ambient temperature to 1000° C with little variation between the different carbon materials. However, graphite exemplified by AGR-graphite has a lower expansion, being less than 0.25% in the same temperature range.

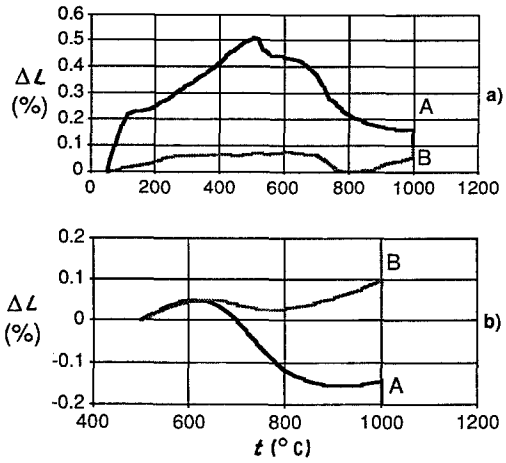

Fig. 3. Thermal expansion/shrinkage of two commercial room temperature ramming pastes. (a) No prebaking. (b) Prebaking to 500° C.

During baking to the operating temperature, paste with coal tar-based binders expands up to about 500° C and then usually contracts. The expansion/shrinkage characteristics depend heavily on the type and granulometry of the filler material, the binder content and quality, the compaction pressure and orientation. Figure 3 gives the dilatometric characteristics of two commercial cold type ramming pastes A and B. These materials were first compacted with a pressure of 10 MPa and their expansion/shrinkage measured in the direction of compaction. The expansion/shrinkage was measured without prebaking (Fig. 3a) and after prebaking to 500° C (Fig. 3b). During the measurements the temperature was increased by 3° C min^{-1} and held at the maximum temperature for 7 h.

When discussing the dilatometric properties it must be noted that a pitch bonded carbon paste remains plastic up to about 500° C. Expansion in the plastic region will not cause any net expansion of the cathode, but the paste will fill possible voids or rise above the seams. We consider the paste shrinkage most realistically evaluated as the shrinkage from around 500° C and up to near cell operating temperature when the sample is baked continuously from room temperature at a rate approximating the temperature increase rate it is likely to experience during cell preheating.

Optimization of aggregate packing density and reduction of the finest fractions reduced room temperature paste shrinkage upon baking, while binder content (within the limits of having a workable paste) has less influence [5]. An illustration of this is given in Fig. 4. Paste I represents the closest packing of the fraction on the assumption of spherical particles, i.e. a straight line with slope −0.5 in the log–log representation in Fig. 4. Paste II is made up of almost equal fractions by weight. In paste III the middle fraction (relative to paste II) is almost removed. This paste may hence be characterized as having a 'two-fraction' granulometry.

3.2. *Sodium intercalation*

The penetration of sodium into carbon blocks usually

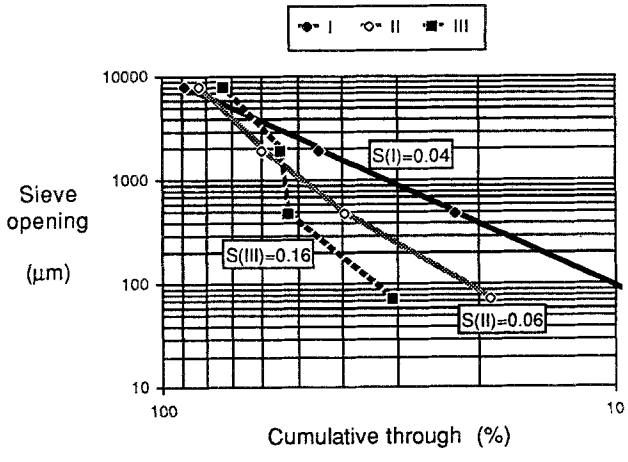

Fig. 4. Examples of experimental room temperature ramming paste granulometries. The shrinkage (S, in %) during baking from 500 to 1000° C is indicated in the boxes (from [5]).

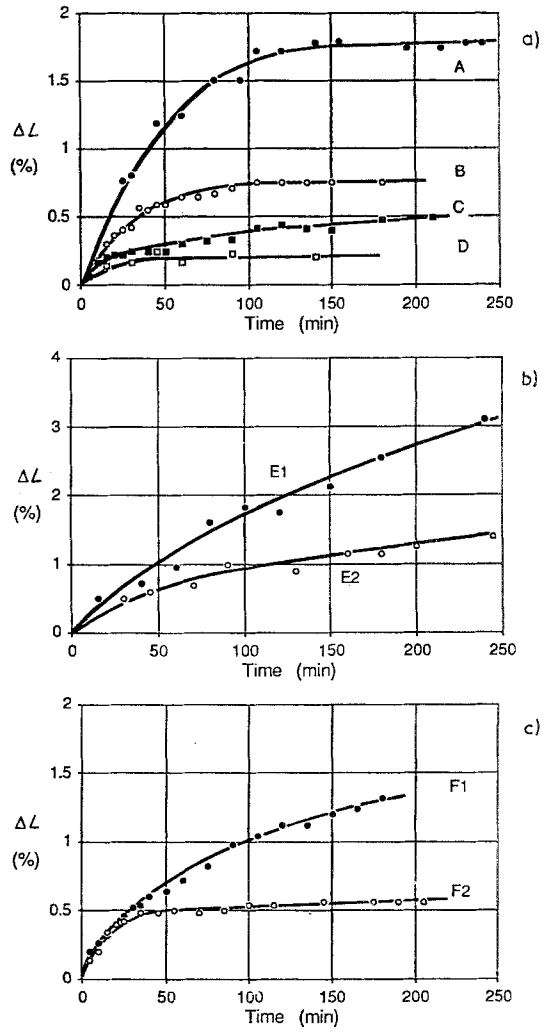

Fig. 5. Expansion due to sodium intercalation of extruded cathode blocks during electrolysis. (a) ECA (A), semi-graphitic (B), semi-graphitized (C) and AUC-graphite (D), CR = 4; t = 960–980° C. (b) Influence of cryolite ratio, CR = 4 (E1) and CR = 2.3 (E2), on an amorphous block, t = 960° C. (c) Expansion of a semi-graphitic block perpendicular (F1) and parallel to (F2) the extrusion direction.

results in an isothermal expansion larger than the total thermal expansion from room temperature to 1000° C.

Figure 5 shows expansion due to sodium intercalation for 5 different commercial extruded cathode blocks and for AUC-graphite. Unless otherwise stated the expansion is measured parallel to the extrusion direction. In a melt with cryolite ratio, CR = 4, amorphous materials typically expand from 1.0 to 3.0% but the expansion can be still higher and complete disintegration may even occur by use of unsuitable materials. The more graphitic materials have a total expansion of 0.5–0.7% while AUC-graphite expands only 0.25% under similar experimental conductions.

When the acidity is increased to CR = 2.3 which is more typical for the industrial electrolyte, the expansion is reduced to about 40% of the expansion of CR = 4 (Fig. 5). This trend is expected due to the lower sodium activity (see Equation 4).

Figure 5 shows the expected increase in expansion perpendicular to the extrusion direction instead of parallel. Extrusion will, especially with graphite, tend to order the graphite flakes parallel to the extrusion

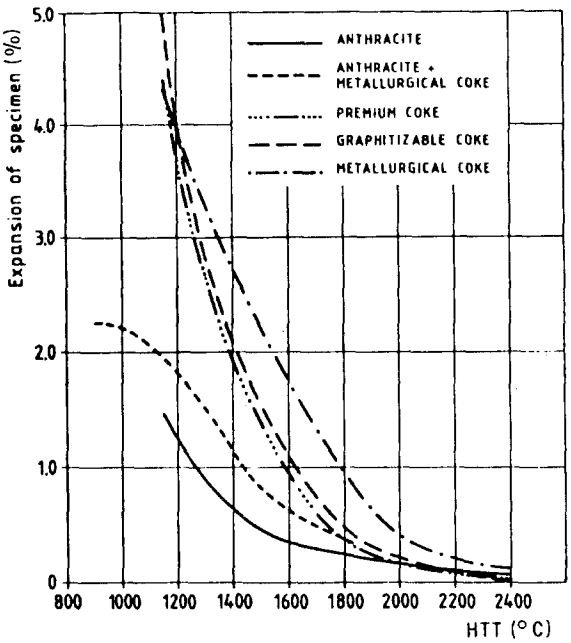

Fig. 6. Cathodic expansion of various types of carbon materials as a function of heat treatment temperature (from [6]).

direction and the largest expansion due to intercalation will be perpendicular to these flakes. This anisotropy in expansion caused by intercalation will be less in pressed and/or vibrated blocks, the expansion parallel to the direction of pressure/vibration (usually vertical during forming) being somewhat higher than perpendicular to this direction.

Wilkening and Busse [6] examined the cathodic expansion of various types of carbon as a function of heat treatment temperature (HTT) and found that anthracite and anthracite-calcined coke mixtures showed less sodium-induced swelling during electrolysis than metallurgical coke and petroleum coke. With respect to anthracite, ECA expanded less than GCA. At HTT above 2000°C little difference was found between the investigated carbon materials (Fig. 6).

3.4. *Cathode heaving*

The heaving of the cathode bottom experienced in industrial cells is believed to be caused by at least two major mechanisms, often operating in concert. One is based on the thermal dilation as well as the sodium-induced swelling of the carbon pane, the other on the formation of columnar crystals or volumetric changes caused by salt penetration or formation within, or beneath, the carbon bottom blocks [7]. Both may result in buckling or warping of the cathode carbon bottom. The magnitude of the heaving is a complex function of several parameters, among which are pot age, lining design, materials, shell strength, start-up and operational practice. Although the heaving rate may be substantially reduced by optimizing some of these parameters some bottom uplift is likely to continue throughout the entire life of the cell, as indicated in Fig. 7.

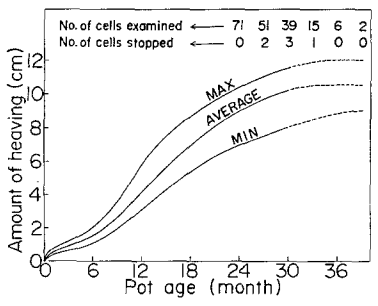

Fig. 7. Pot lining uplift measured in operating cells (from [7]).

Thermal and Na gradients typically occur during preheating of the cell and during start-up when sodium progressively intercalates from the top. If the gradient in the vertical direction is assumed linear, the maximum heaving (maximum deflection, δ) of an unrestrained block due to thermal and intercalation effects is given by [8]:

$$\delta = (\alpha_{Na} l^2 \Delta C_{Na} + \alpha_\tau l^2 \Delta t)/(8h) \qquad (14)$$

where α_{Na} and α_τ are the sodium and thermal expansion coefficients, while ΔC_{Na} and Δt are the concentration and temperature differences, respectively. This equation states that, with a bottom block length $l = 280$ cm and a height $h = 45$ cm, a 1.5% expansion on top due to sodium intercalation results in a 3.3 cm deflection.

Large pockets or voids, often filled with crystallized bath components, are sometimes found deep inside used pot linings. The formation of salt lenses in the cathode resembles the 'frost heave' phenomenon caused by freezing of water in porous soils, as described by Everett [9]. The resulting damage has not necessarily any connection with the expansion which occurs when water freezes, as similar damage can be inflicted by liquids that contract upon freezing. What takes place is a preferential growth of crystals in the larger pores of a porous solids. If a supercooled liquid begins to freeze, both in a fine pore and in an interconnected large pore, crystal growth in the small pore will be limited by the pore space in which it is contained. Once a difference in size has been established between crystals, the larger crystals will grow at the expense of the smaller.

4. Characterization of cathode materials

Proper start-up procedures and operation are extremely important for a satisfactory life of a cell, but the thermomechanical and chemical properties of cathode materials relative to the design of the lining may lead to failure in an otherwise normally operated cell. The producers of cathode materials (carbon blocks, ramming paste, firebricks and insulation) usually characterize their materials well with respect to room temperature properties but it is also important to have a good understanding of materials properties under actual start-up and electrolysis conditions. Towards this goal we have adapted, improved or developed the following test methods which we consider important as design tools as well as for quality control of the materials [10]: (1) thermal expansion/contraction of carbon blocks; (2) thermal expansion/

contraction of ramming pastes; (3) thermal conductivity of carbon blocks at elevated temperatures; (4) abrasion resistance of carbon during electrolysis; (5) compaction characteristics of ramming pastes; (6) aluminium carbide formation; (7) oxidation resistance of carbon; (8) fluoride resistance of refractory and insulation materials; (9) expansion of carbon due to sodium penetration; (10) rate of sodium penetration in carbon; (11) chemical resistance of carbon towards sodium; (12) characterization of graphitization by X-ray diffraction; (13) characterization of graphitization by electron acceptor intercalation.

Some results have already been given (from methods 1, 2 and 9). A complete description of the test methods will not be given, but some of the most relevant methods are summarized in the following, i.e. methods 1, 2, 5, 9, 11 and 12.

4.1. *Thermal expansion/contraction of blocks and seam mix during baking*

In order to measure the thermal expansion/contraction during baking, the samples (40 mm diameter × 50 mm) are to approximately 1500 kg m^{-3} at a temperature in the middle of the temperature window obtained by the tampability tests (see later). The test specimens are heated at a rate of 180° C h^{-1} from 20° C to 940° C. The samples are held at the top temperature for 7 h. The block samples are not baked but simply drilled out of blocks. The expansion/contraction is followed by a fully automated computer system, and measured relative to 50° C. The experimental set-up is shown in Fig. 8. Examples of results are shown in Fig. 3.

4.2. *Compaction characteristics (only for paste)*

As a ramming tool a +GF+ Sand Rammer Type PRA (George Fischer Ltd, Schaffhausen, Switzerland) is used. The compaction takes place as the energy from a falling weight is transferred to the paste (180.0 g paste in a 50 mm steel cylinder) through a piston resting on the paste. The energy of each stroke is independent of the degree of compaction, i.e. the height of the paste cylinder. This height (H) can be read directly to the nearest 1/10 mm after each stroke and the paste density (ϱ) is computed:

$$\varrho = k/H \tag{15}$$

where k is a constant determined by the mould geometry and the weight of the ramming paste in the mould. The compaction is performed in a standardized manner with up to 350 strokes or number of rammings (N). The height of the cylinder is most frequently read at low N, less frequently as the number of strokes increase.

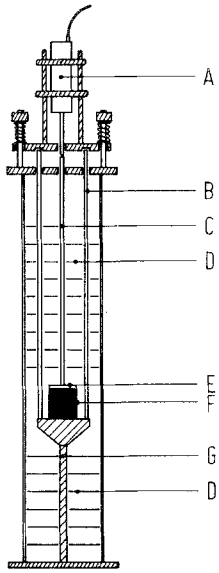

Fig. 8. Experimental set-up for expansion/contraction during baking. (A) Transducer, (B) quartz tubes for transducer support, (C) quartz tube which transfers the expansion/contraction to the transducer, (D) radiation shields, (E) quartz plate, (F) test specimen, (G) supporter.

In order to examine the temperature sensitivity of the pastes, the compactions are performed at three different temperatures: for instance 10, 20 and 50° C or 35, 65 and 95° C. The paste, steel cylinder, pedestal and piston have to be cooled or heated to the given temperature, respectively, by circulating water around the steel cylinder. Figure 9 shows some compaction curves.

To characterize the tampability of the different pastes, the curves are curve-fitted to a three-parameter (α, β, γ) cumulative Weibull distribution function:

$$\varrho = \varrho_{\max} - \Delta\varrho \exp\{-[(\log N - \gamma)/\alpha]^{\beta}\} \tag{16}$$

The pre-exponential factor, $\Delta\varrho$, equals $\varrho_{\max} - \varrho_0$ where ϱ_0 is the lower asymptotic value, which may represent a loose (gravimetric) compaction of the paste. The parameters have the following physical significance:

log N: base 10 logarithm of the number of rammings (N);

α the scaling or normalization parameter which determines the steepness of the curve (decreases as α increases);

β the Weibull modulus, or shape parameter, which controls the asymmetry of the distribution;

γ the location parameter which has the effect of shifting the origin of the distribution.

The fit is nearly independent of the Weibull shape parameter if $\beta > 3$ and β is chosen equal to 6.

The number of rammings (N_2) which gives the minimum value of the second derivative of ϱ (with respect to log N) (third derivative = 0) is calculated:

$$\begin{aligned}\varrho''' = {} & \Delta\varrho(\beta/\alpha^3)[\beta^2((\log N - \gamma)/\alpha)^{(3\beta-3)} \\ & - \beta(3\beta - 3)((\log N - \gamma)/\alpha)^{(2\beta-3)} \\ & + (\beta - 1)(\beta - 2)((\log N - \gamma)/\alpha)^{(\beta-3)}] \\ & \times \exp\{-((\log N - \gamma)/\alpha)^{\beta}\} = 0\end{aligned} \tag{17}$$

A Newton–Raphson iteration method is used:

$$N_{n+1} = N_n - \varrho'''/\varrho'''' \tag{18}$$

For our set-up, pastes with N_2 values less than 65 are considered too 'wet' to be compacted while pastes

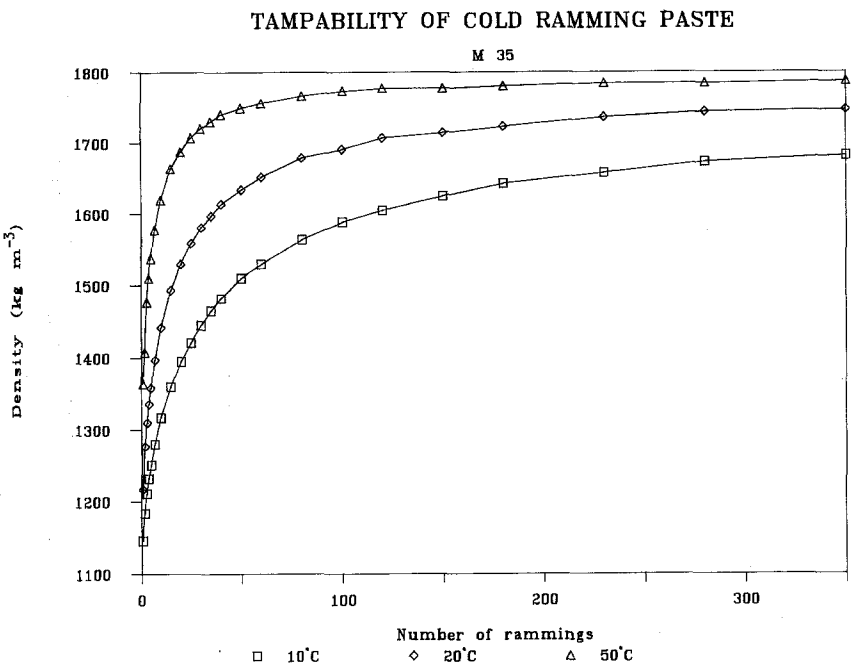

Fig. 9. Tamping characteristics of a cold ramming paste.

with N_2 values higher than 130 are estimated to be too 'dry' to compact properly at a given temperature. 'Normal' pastes are assigned N_2 values between 65 and 130, with borderline cases on each side of this range. These values are arrived at by calculation of $\varrho''' = 0$ for the samples studied in an earlier paper [11]. Based on the criteria that N_2 should be between 65 and 130, and using a plot of log (N_2) vs log K, the temperature windows are calculated. This window is found to be between 21 and 33° C for the ramming paste shown in Fig. 9.

4.3. *Sodium expansion/modified Rapoport test*

The Rapoport or modifed Rapoport test [12] is a differential method for precisely measuring the linear expansion due to sodium penetration of a baked carbon sample during electrolysis of aluminium.

A Sylvac position metering probe connected to a Sylvac digital indicator unit (D50P, FRG) with an accuracy of 1 μm, is used to observe the change in the position of the edge of a hollow stainless steel tube, which is an extension of the cylindrical specimen. The change in position is determined relative to a boron nitride rod which, in turn, monitors small changes in the position of the cell components caused by the harsh conditions encountered during electrolysis.

Discussions with different laboratories made it clear that the classical Rapoport test does not function well and therefore is not often used. In order to avoid some of the problems inherent in the Rapoport test, we choose to monitor the expansion in an open system under an argon atmosphere, with a boron nitride rod as our fixed reference. Using this technique we are able to show the effect of cryolite ratio and choice of cathode material on expansion during electrolysis.

A schematic diagram of the apparatus is shown in Fig. 10. The cathode is a vertical cylinder of carbon material, 25 mm in diameter and 60 mm long, with a hole through its centre parallel to the long axis. A boron nitride rod, slightly thinner than the diameter of the hole and attached to the centre of a boron nitride disk, 10 mm thick and 50 mm in diameter, is then inserted into the cylindrical cathode making the bottom face of the cathode rest on the boron nitride disk. Surrounding the boron nitride rod and resting on the upper surface of the cathode is a hollow stainless steel tube. This tube becomes an extension of the cylindrical cathode and conducts current from the power supply to the cathode. The upper part of the

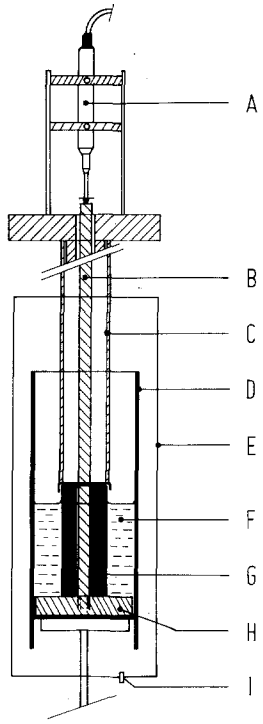

Fig. 10. Apparatus for a modifed Rapoport test. (A) Position metering probe, (B) boron nitride rod, (C) Inconel steel cathode extension, (D) graphite crucible (anode), (E) furnace, (F) cryolite melt, (G) ramming paste test specimen (cathode), (H) boron nitride plate, (I) gas inlet.

tube supports the Sylvac probe, which measures the difference between the height of the upper edge of the tube and the upper surface of the boron nitride rod. This difference gives the expansion or contraction of the cathode.

This electrolysis configuration is, in effect, perpendicular to the usual industrial configuration because electrolysis occurs on the cylindrical surface of the cathode and the inside surface of the crucible anode walls.

Because the system is open, some sodium and bath evaporate over the course of an experiment and the effective length of the carbon cylinder is continuously reduced from an initial height of 50 mm to approximately 46 mm at the end of the experiment. As most of the expansion occurs during the first hour of electrolysis and some wetting of the cathode can be assumed, the expansion is calculated with respect to a cathode height of 50 mm. Since the geometries of all of the parts of the assembly are fairly regular and the density of the molten salt mixture is very close to 2.1 g cm^{-3} over the temperature range of interest, it is a simple matter to weigh out the exact amount of salt needed to fill the crucible to any predetermined level.

4.4. *Sodium vapour resistance*

For the sodium vapour resistance test Na (p.a.) is used. For blocks drilled out of cylinders are used while the ramming pastes are pressed at room temperature to the same size (15 mm × 30 mm) and baked to 1000° C with a heating rate of 80° C h^{-1}. The samples are then kept at 1000° C for 12 h.

The reactor for the testing of the ramming pastes consists of the stainless vessel shown in Fig. 11. The top of the vessel is outside the hot zone in the furnace.

Test specimens and sodium metal are transferred to the steel vessel in an argon atmosphere drybox, where the levels of O_2 and H_2O are kept below 5 ppm. The closed vessel is placed in a vertical Marshall furnace and the vessel evacuated to an Ar pressure of 100 Torr. The temperature is raised to 800° C over a period of 1.5 h making the pressure increase from 100 to 500 Torr. The samples are kept at 800° C for 4–4.5 h before they are allowed to cool overnight. The pressure then decreases to the initial value, 100 Torr. The specimens are then taken out and classified as: extreme cracking, heavy to moderate cracking, hairline cracks, little damage, no effect.

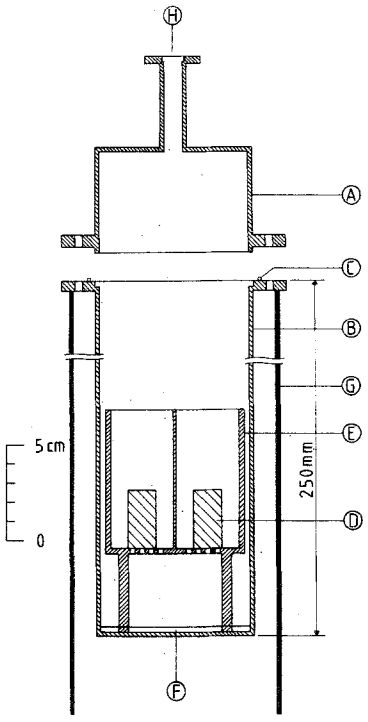

Fig. 11. Apparatus for sodium vapour test. (A) Lid, (B) container, (C) gold gasket, (D) carbon specimen, (E) sample holder, (F) sodium metal (liquid), (G) furnace, (H) to manometer.

4.5. *X-ray characterization*

X-ray characterization of baked ramming pastes is made from powder diffraction data using the (002) diffraction peak of graphitic carbons. An intensity ratio of peak height relative to a natural Skaland graphite is calculated, using identical recording conditions. CS49 graphite is used as a secondary standard with an intensity ratio of 0.55. This intensity ratio is a good measure of the amount of graphite in the sample.

5. Cell failure due to materials

As already pointed out, proper start-up and operation are extremely important for a satisfactory life of an aluminium cell. Nevertheless failures may also be due to materials properties. A comprehensive discussion of failure mechanisms is given in [10] and only some of the most important failures due to materials properties and/or design will be mentioned here in conclusion.

5.1. *Improper heat balance*

The thermal conductivity of the materials and the amount and quality used must give isotherms in proper locations. The bath freezing isotherm (≈ 780° C) should be just below the carbon blocks. A freezing isotherm inside the carbon blocks may result in frost heave damage, and a freezing isotherm too far down into the refractory/insulation layer results in damage of the insulation layer, which is usually less dense and less salt resistant then the upper refractory layer. The thermal conductance of the sidewalls should result in a proper frozen ledge.

5.2. *Improper collector bar design and mounting*

Cracks may proceed from the joints between the collector bar and the carbon due to improper mechanical design or joining techniques. Then molten aluminium can penetrate through the carbon, disturbing the heat balance and finally destroying the cell.

5.3. *Improper ramming*

The ramming paste should be rammed within the temperature window which gives optimum compaction.

5.4. *Excessive shrinkage of ramming paste between 500 and 1000° C*

Shrinkage of ramming paste after it has become non-plastic may give cracks where aluminium can penetrate. Failure caused by improper ramming or choice of paste is one of the most common reasons for pot failure.

5.5. *Too low sodium resistance of the carbon materials*

Low sodium resistance may lead to spalling or deterioration of the carbon materials. Low sodium resistance is also usually accompanied by high sodium expansion which may give excessive expansion and heaving.

5.6. *Oxidation of sidewalls*

Oxidation of sidewalls may be the limiting factor of an otherwise properly constructed cell. Good protection against oxygen or use of more oxidation-resistant materials is necessary.

5.7. *Reaction between fluorides and refractory*

The fluoride bath will penetrate into the refractory/insulation layer and, if the fluoride resistance of these materials is too low, they may deteriorate completely and lead to disruption of the cathode bottom.

5.8. *Deformation of steel shell*

The strength and stiffness of the steel shell decrease during its years in service. A relining of a previously used cathode is, therefore, performed in a casing which, in addition to possible deformations, is weaker than when it was first put into service. This may reduce the support it contributes to the lining materials and, thus, the structural integrity of the lining itself. The net effects may be more rapid deformations and shorter pot lives. Modern cathodes are designed with steel shells that may be rigid enough to withstand the forces that act upon them, or with shells that become mostly elastically deformed. With rigid shells, compressive zones have to be built into the lining to prevent cracking of the carbon.

Acknowledgement

We wish to express our gratitude to Elkem a/s & Co, Mosal Aluminium for permission to publish. The work has also been supported by NTNF in cooperation with the Norwegian aluminium industry.

References

[1] G. J. Houston and H. A. Øye, *Aluminium* **61** (1985) 251, 346, 426.
[2] W. L. Worrell, *Can. Met. Quart.* **4** (1965) 87.
[3] K. Grojotheim, R. Næumann and H. A. Øye, *Light Metals* (1977) 233.
[4] H. Kvande, Thermodynamics of the system NaF–AlF_3–Al_2O_3–Al studied by vapour pressure measurements. Dr. Techn. Thesis, Institute of Inorganic Chemistry, Norwegian Institute of Technology, University of Trondheim (1979).
[5] S. R. Johansen, MSc. Thesis, Institute of Inorganic Chemistry, Norwegian Institute of Technology, University of Trondheim (1987).
[6] S. Wilkening and G. Busse, *Light Metals* (1981) 653.
[7] T. Watanabe, H. Hayashi and F. Muchizuki, *J. Metals* **20** (1968) 64.
[8] S. Wilkening, Third Aluminium Workshop – Hall-Heroult Cathodes, Carneige-Mellon University, Pittsburgh, PA, Feb. (1987).
[9] D. H. Everett, *Faraday Soc.* **57** (1961) 1514.
[10] M. Sørlie and H. A. Øye, 'Cathodes in Aluminium', Aluminium Verlag, Düsseldorf (1989).
[11] M. Sørlie and H. A. Øye, *Light Metals* (1987) 571.
[12] D. S. Newmann, O. T. Dahl, H. Justnes, S. Kopperstad and H. A. Øye, *Light Metals* (1986) 685.